

On the Thermographic Analysis and Thermal Resistance Estimation of the Capacitor-Run Single-Phase Induction Motors

Danila Adrian* and Campeanu Radu Mihai†

* Transylvania University of Brasov/Department of Automation and Information Technology, Brasov, Romania, adrian.danila@unitbv.ro

† Transylvania University of Brasov/Department of Automation and Information Technology, Brasov, Romania, radu.campeanu@unitbv.ro

Abstract - The real-time estimations of heating of the electromechanical converters are important for both overheating prevention and overall efficiency optimization during operation. The two-phased induction motors with capacitor-run capacitors onto the auxiliary phase are sensitive to the capacitance variations of the capacitor. In this respect, the optimization of the two-phased induction motors with electronically-switched, capacitor-run, supplied from frequency inverters may be achieved if the elliptical magnetic motion field into the machine is controlled such as the ratio between the maximum and the minimum of its amplitude is reduced to unity. Observations of the heat of the machine's body and an appropriate thermal model may provide information about the eccentricity of the magnetic motion field in the machine. In this work, the authors investigated the impact of the capacitor-run capacitance onto the characteristics of the thermal field of the machine. In this perspective, the authors implemented a method based on the image analysis techniques that allows estimating: (a) the geometric features of the machine from the boundaries of the thermal field, and (b) the temperature distribution onto the cross-section of the body in correlation with the main components of the machine and (c) the thermal resistance of the machine's body.

Cuvinte cheie: analiza imaginilor, analiza câmpurilor de temperatură, motoare asincrone bifazice cu condensator.

Keywords: image analysis; thermographic analysis; capacitor-run two-phase induction motors.

I. INTRODUCTION

The thermal processes within the electromechanical converters such as electrical transformers and electrical machines are well documented within literature, [1], [2]. Nowadays, thermovision apparatus such as thermal cameras and pyrometers are available as contact-less, large bandwidth, portable devices. In correlation with the implementation of field's analysis software these thermovision apparatus made possible implementing observations of the thermal processes into the electromechanical converters during their operation, Fig. 1. This implementation is important for fault detection, [3] and process's efficiency optimization, [4].

From the theoretical point of view, the thermal processes into electrical machines are distributed-parameter processes depicted by partial differential equations involving the Fourier's heat equation.

For example, an insight into the thermal processes in the electrical transformer and the DC machine, made by means of the Finite Elements method, [4] is straightforward if the entries – field geometry, material constants, initial conditions and boundary conditions are well estimated. For the induction machine, however, this approach is more difficult due to: the rotating rotor, the unobservable rotor currents and the nonlinearity of the dynamic model of the process. In this case, the online process identification with process-in-the-loop adaptive models is more suitable.

In a previous published paper, [5] the author investigated two methods for estimating the power losses and the un-observable currents into the squirrel-cage rotor of the induction motor by means of thermo-vision analysis.

In this paper, the authors extended the analysis presented in [5] for the case of the capacitor-run, two-phased induction motor in two cases: (1) the capacitor-run capacitance at it's the factory value and, (2) the capacitor-run capacitance is altered at a lower value. The aim of the investigation is to provide estimations of the thermal resistance of the motor's body and of the impact of the capacitor-run capacitance on the power-losses of the machine.

The organization of the paper is the following. In Chapter II, the theoretical background, the main steps of the method and the software routines are presented. In Chapter III, the experiment implementation and the results are detailed.

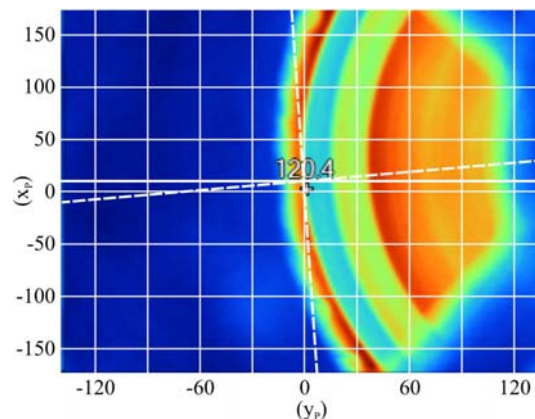


Fig. 1. Example of the thermal spectrum on the cross-section of the test-unit, acquired with the thermal camera.

In Chapter IV the analysis of the results is presented and discussed. The conclusions of the report and further developments of the work are presented in the final chapter of the paper.

II. METHODS

In this chapter the background of the thermal models of the electrical machines, the methods and algorithms used in image processing for noise reduction and systematic-errors processing of images, the geometric features detection and field analysis are presented.

A. The Thermal models and the Thermal Resistance of the electrical machines

In the literature, [1], the thermal processes in the electrical machines are depicted by means of two simplified models: (a) the model of the unique body and (b) the two bodies' model. The unique body model is suitable for the symmetrical structures such as the induction machines; the two bodies' model is suitable for the asymmetrical structures such as for the DC machine or the synchronous machines.

In detail, the sources of heat during the operation of the induction machine are located in two distinct areas: the stator's windings and the rotor's windings. The heat produced in the machine, diffuse through the bodies of the stator and rotor by thermal conduction and to the cooling environment – the air – by convection and thermal radiation. The heat transfer from the heat sources to the cooling environment may be observed by means of the temperature distribution upon the cross-section of the machine during the machine's operation.

Form the balance of power in the electrical machine one may write the following expression.

$$P_1 = P_m + P_J + P_{hist} + P_{fr} \quad (1)$$

Where: P_1 is the total input power, P_m is the mechanical power at the machine's axis, P_J are the power losses in the machine's windings due to the Joule-Lenz effect and the skin effect, P_{hist} is the magnetic hysteresis power losses and P_{fr} are the power losses due to the friction. The term P_J has the major impact over the heating of the machine.

For experimental purposes, in the expression (1) the terms P_1 , P_m are observable by measurements, the term P_{fr} may be estimated by investigation of the free-braking of the drive and the term P_{hist} may be included into the thermal power losses. Thus, the expression (1) gives an overall estimate of the thermal losses of the machine.

The thermal energy produced in a given interval of time, dt , equals to $P_J \square dt$; it has two components: the first component, dQ_{body} is the amount of thermal energy of the body of the machine that determines the increase of its temperature and the second component, dQ_{trsf} is the amount of thermal energy transferred to the environment by thermal radiation.

In the unique body's model the following hypotheses are assumed (for simplification purposes).

(a) The entire body of the machine is isotropic and homogenous.

(b) The heat source is located at center of the body.

Although, the thermal conduction, convection and radiation processes evolve differently, for the usual range of temperature (from 0 °C to 250 °C) one may assume simplified expressions for the terms dQ_{body} and dQ_{trsf} and the expression (1) writes as follows.

$$P_J dt = m \cdot c d\theta + S \cdot \alpha \cdot \theta dt \quad (2)$$

$$C_T \cdot \frac{d\theta}{dt} + \frac{1}{R_T} \cdot \theta = P_J; \quad \theta|_{t=0} = 0. \quad (3)$$

In the expressions (2) and (3) θ is the increase of temperature of the body, m is the mass of the body, c is the equivalent specific heat, S is the cross-section surface of the body, α is the equivalent coefficient of the thermal transmission, $C_T = m \cdot c$ is the thermal capacitance of the body, and $R_T = 1/(\alpha \cdot S)$ is the thermal resistance of the body.

The solution of the first-order, linear differential equation (3) is then given by the following expression:

$$\theta(t) = \theta_m \cdot \left(1 - e^{-\frac{t}{T_f}} \right) \quad (4)$$

In the expression (4), $\theta_m = R_T \cdot P_J$ represents the stationary increase of temperature of the body. The thermal resistance (as well as the thermal capacitance) is specific for the electrical machine itself and thus their estimates may be used in quality testing, faults detection during operation and dynamic control.

B. Processing of the Thermal Field Images

In contrast with the computed thermal field, which matches to the shapes of the target, the thermal field images - captured from real-life experiments by means thermal cameras, are blurred and corrupted by the margin noise. The processing of the images, [6] aims to minimize these items. The main approach in preprocessing an image is threshold and filtering of the image. Before threshold, colored images are transformed into gray-scaled images.

The thermal field image of a thermal process depicts the values of a unique variable – the temperature – therefore is not gray-scaled before threshold. In this case, threshold is referred to the arrangement the temperature values of the field into bins of increasing values and to the transformation the given field into a stairs-like field. In this approach, the smooth variations of the temperature within each bin are equivalent with constant values without losing the information related to the geometric shape of the field.

The procedure described in [5] allows to reduce the number of regions at around a given temperature and to estimate the analytic representation of boundaries. In order to estimate the geometric features of the field, such as the analytic expressions of the basic shapes,

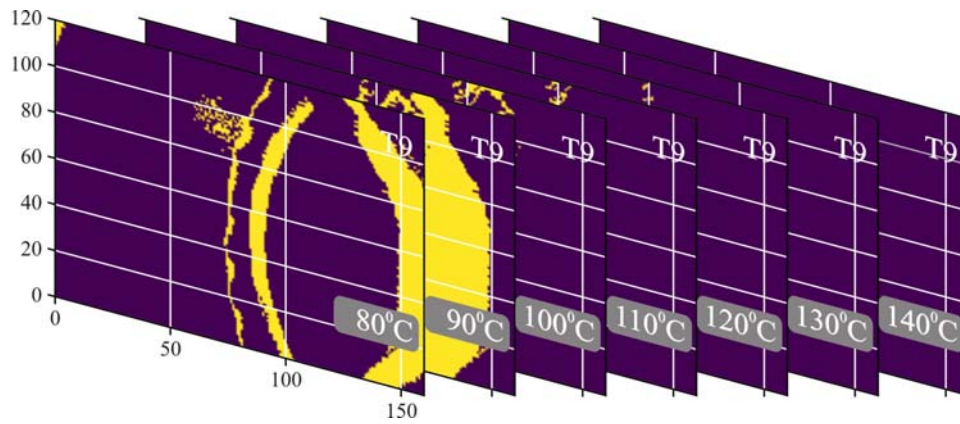


Fig. 2. The threshold images are spread into images of the corresponding to threshold values. Example: the components of a thermal field image.

the boundaries or the surfaces of regions at given temperature, the stairs-like image at each level of temperature of the field must be split into two-level images - a two-level image for each level of temperature, Fig. 2.

The two-level images are straightforward to convert into binary images and filtering without losing the information about the boundaries and regions of the thermal field.

In this paper we implemented the software applications described in [5] for the calibration of the images and the geometric feature detection from images of the thermal spectra. The proposed method is based on the Radon transformation algorithms and the Kása and Coope method, [7] for circle and ellipsis detection onto the scene. The geometric features of interest in these experiments were: the coordinates of the center and the radius of the circle in the image representing the shape of the stator of the electrical machine, Fig. 3.

C. Segmentation and Feature detection

With image segmentation one may group the pixels of the image into regions according to pre-defined pattern or criteria. The regions are labeled for indexing and then various features of indexed regions - such as surface, position of statistical momentums, etc. - may be estimated. The steps to follow in this experiment were:

(1) Marking the pixels from the binary image according to their intensity.

(2) Defining the patterns of regions to label.

(3) Labeling the marked regions according to the patterns.

(4) Estimating the surface of each labeled region.

(5) estimating the sum of the pixels of all regions at a given temperature.

In the Python ecosystem, these actions were made with the modules *skimage* and *scipy*, [8].

The results are arrays where each unique feature in the input has a unique label and the number of labeled objects found.

In Fig. 4, the image of the labeled regions for a given test is depicted.

D. Temperature distribution analysis

In the experimental analysis of the temperature distribution on the cross-section of the machine doesn't vary monotonically over the surface of the cross-section.

Therefore, the estimation of the stationary increase of temperature, θ_m was by averaging over the true distribution onto the surface, i.e. with the expression:

$$\theta_m = \frac{\sum_{i=1}^N \theta_i \cdot S_i}{\sum_{i=1}^N S_i} \quad (5)$$

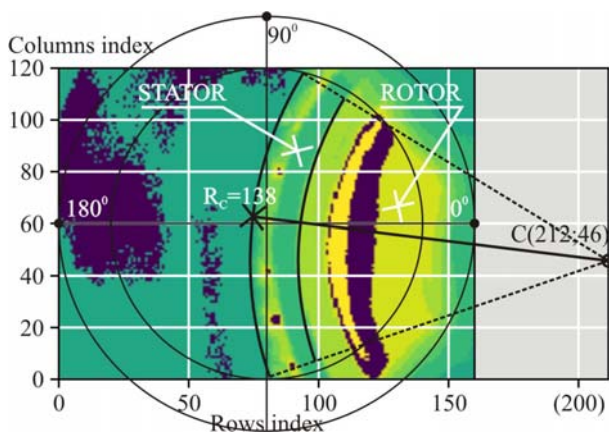


Fig. 3. The estimations of the coordinates of the centre and of the boundaries of stator and rotor onto the thermo-graphical image of the test-unit, [7].

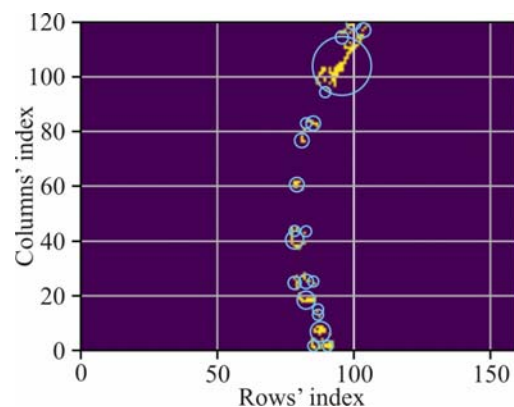


Fig.4. An example of segmentation for the 110 °C component at the T0 test.



Fig. 5. The test-unit on the experimental test-bench.

In the expression (5), θ_i is the temperature level at the region of area S_i . N is the number of regions onto the cross-section surface of the electrical machine.

III. THE EXPERIMENT

The goals of the experiments made in this work were to provide a method for estimating the value of the equivalent thermal resistance of the electrical machine and to study the impact of the deviations of the capacitor-run capacitance onto the power-losses of the drive.

The experiment was made by means of the followings hardware and software.

The test-unit: 2-Phase, capacitor-run, squirrel-cage induction machine of type MSP311.

The electrical specifications are given in Table I and the geometrical features are given in Table II.

The breaking unit - a powder-brake of type Magtrol 2PB43. The technical specifications are given in Table III.

The infrared camera - of type Fluke T120. The technical specifications are given in Table IV.

TABLE I. THE ELECTRICAL MACHINE OF TYPE MSP311 – ELECTRICAL AND ELECTRO-MECHANICAL FEATURES.

No.	Electrical and Mechanical Features (extract)		
	Denomination	Value	Units
1.	Input voltage	230	V
	Phase currents	1.9/1.45	A
2.	Rated frequency	50	Hz
3.	Rated angular speed	2840/420	rpm
4.	Number of pair-poles	-	2/12
5.	Mechanical power	611	W
5.	Start-up capacitance	μF	14

TABLE II. THE ELECTRICAL MACHINE OF TYPE MSP311 – GEOMETRICAL DIMENSIONS.

No.	Geometrical Dimensions (extract)		
	Denomination	Value	Units
1.	Stator's outer diameter	154	mm
2.	Stator's inner diameter	$93^{+0.1}$	mm
3.	Rotor's diameter	$93_{-0.03}$	mm
4.	Slots' depth	16.85	mm

TABLE III. THE POWDER BRAKE 2PB43.

No.	Electromechanical Features (extract)		
	Denomination	Value	Units
1.	Rated torque	10	$\text{N}\cdot\text{m}$
2.	Rated power	1	kW
3.	Rated angular speed	955	rpm
4.	Max. angular speed	4000	Rpm
5.	Measurement unit	DSP6001	-

TABLE IV. THE INFRARED CAMERA T120.

No.	Technical Specifications (extract)		
	Denomination	Value	Units
1.	Temperature measurement range	-20 to 650	$^{\circ}\text{C}$
2.	Measurement accuracy	2	%
3.	Minimum span	2.0	$^{\circ}\text{C}$
4.	Total pixels	30,000	-
5.	Software	SmartView	-

General purpose apparatus: two electronic voltmeters (range 0 to 500 V, accuracy 3%) and 2 magneto-electric ampere-meters (range 0 to 5 A, accuracy 1%).

The software implementations used the modules from the Python environment *numpy*, *scipy*, *os*, *skimage* and *matplotlib*.

The experiment hardware is presented in the Fig 5. The experiment organization was as follows.

Step 1. The test-unit had run 30 minutes in no-load operation for thermal conditioning; then, the braking torque has been applied in steps up to the rated torque. Observations were made upon 18 values of the torque. Each time the braking torque changed, the test-unit had run another 30 minutes for thermal conditioning before the measurements. Then, the input power, the angular speed and torque, and a thermo-graphical image were acquired.

Step 2. (a) The acquired thermo-graphical images were preprocessed and the 126 images were drawn up for the analysis.

(b) The background image was used for calibrating and scaling images.

(c) The areas of regions corresponding to the prescribed levels of the temperature were estimated and the data was prepared for the next step.

Step 3. The data from the previous steps were assembled and processed. The thermal power losses were estimated from data at Step 1.

From the thermal profile of the spectra at Step 2, the coordinates of the axis of symmetry and the radius of the body of the motor onto the image were estimated. Then, the regions corresponding to the rotor, stator and the air gap of the machine were identified.

From data at Step 2, the increase of the body's temperature was estimated. The equivalent thermal resistance was evaluated by computing the regression line in the least-squares sense.

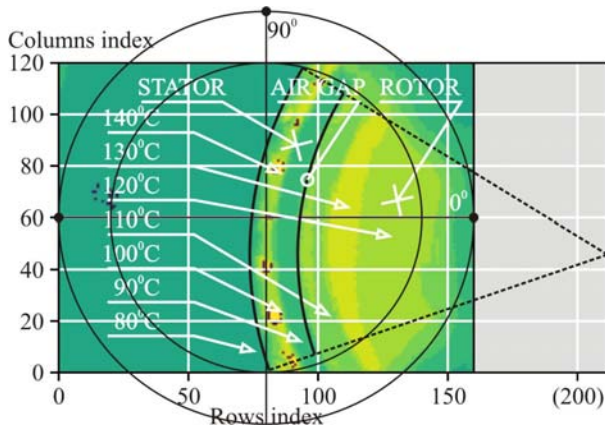


Fig. 6. The mapping of regions at equal temperature levels over the main parts of the electrical machine.

Step 4. The above procedure was implemented twice, for two values of the capacitor-run capacitance: at the factory value, $C = 14 \mu\text{F}$ and at an altered value of $C = 11 \mu\text{F}$. The results were compared and interpreted.

IV. RESULTS AND DISCUSSION

The estimated coordinates of the center of the machine's body cross-section - referred to the origin of the coordinate system of the image, the angle between the axes and the boundary of the rotor were estimated, as depicted in Fig. 3. This action was detailed in [5].

A. The localization of regions per temperature levels

The localization of regions per temperature levels is depicted in the Fig. 6. The results prove that the maximum of temperature is located at the bottom of the stator slots and inside the rotor, near the surface of the rotor.

The temperature increase at the bottom of the slots concerns the stator windings and determines an additional increase of its equivalent resistance. This increase adds to the resistance increase due to the skin effect.

Referring to the rotor, the increase of temperature inside the rotor body, determines an increase of its equivalent resistance and a space distribution of the induced currents onto the cross-section of the squirrel-cage which is similar with the skin effect.

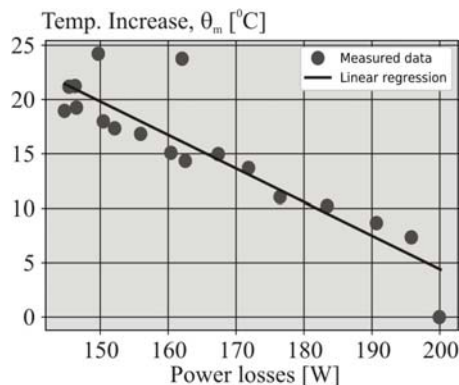


Fig. 7. Case 1 - $C = 14 \mu\text{F}$. The dependency between the increase of temperature of the machine's body and the power losses in the machine.

TABLE V. THE THERMAL RESISTANCE ESTIMATIONS.

No.	The Thermal Resistance Vs Increase of Temp. (extract)			
	θ_m [°C]	R_T [°C/W]	R_{T_Est} [°C/W]	Errors [%]
1.	7.353	0.037	0.029	28.950
2.	15.091	0.094	0.103	9.178
3.	24.220	0.161	0.132	21.644
Avg.	15.341	0.097	0.098	16.816

B. The impact of the capacitor-run capacitance on the temperature increase of the motor's body

To evaluate the impact of the deviations of the capacitance onto the thermal regime of the electrical machine, the procedure depicted in Chapter III was implemented in to two separate cases. Case 1, the value of the capacitance of the capacitor-run was set at $C = 14 \mu\text{F}$ - the factory value and, Case 2, the value of the capacitance was altered to $C = 11 \mu\text{F}$.

In Fig. 7, the experimental measurements are grouped near their linear approximation. This result proves that, the temperature increase and the power losses into the machine are closely cross-correlated. The temperature increase varies proportional with the power losses of the machine and with the load. In this case, the magnetic motion field in the machine is almost circular. The proportional coefficient above is the thermal resistance of the machine's body. The estimations of the thermal resistance are given in Table 1.

In the following, the procedure was implemented for Case 2. The results, presented in Fig. 8, prove that the temperature increase and the power losses are less correlated than the results in Fig. 7. The regression line is almost horizontal and the variance of the samples is higher. The increase of the temperature range is between 3 to 11 °C, i.e. the body's temperature is almost constant with the load. This phenomenon is due to the stationary component of the elliptical magnetic motion field that continuously heats the body.

Thus, the power losses computation from the balance of power in the electrical machine doesn't match to the thermal process. This result is important in the frame of the variable speed control of the electronically commutated switch -capacitor of the two-phased induction motor supplied from frequency converters.

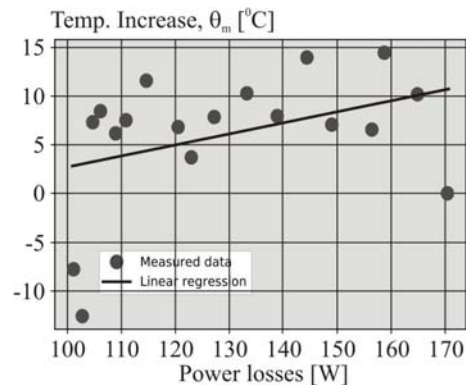


Fig. 8. Case 2 - $C = 11 \mu\text{F}$. The dependency between the increase of temperature of the machine's body and the power losses in the machine.

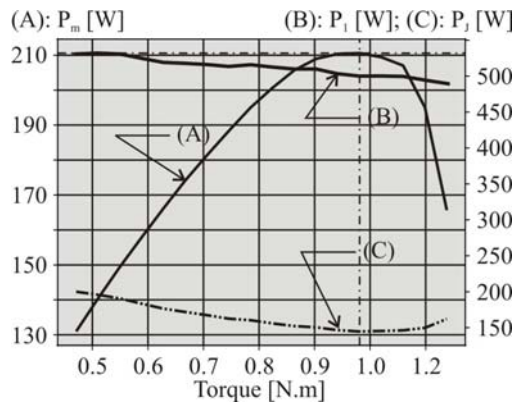


Fig. 9. Case 1 - $C = 14 \mu\text{F}$. The graphs of the mechanical power - P_m , the input power - P_i and the thermal power-losses - P_j versus the load's torque from the experimental measurements.

C. The impact of the capacitor-run capacitance on the power components

The dependencies between the input power, the mechanical power and the thermal power losses with respect to the torque are depicted in Fig. 9 and 10.

In the Case 1, as expected, the mechanical power has a peak nearby the rated torque. In the Case 2 instead, one may observe that the peak of the mechanical power corresponds to the 0.94 N.m. This is slightly less than 0.98 N.m resulted from the natural mechanical characteristic. During the experiment, we remarked that, at the rated torque the machine suddenly stopped. The range of the input power and the power losses are slightly lower in comparison with the case 1.

V. CONCLUSIONS

The method investigated in this work allows obtaining an insight of the thermal processes during the steady-state operation of the capacitor-run, two-phased induction machines.

The image processing-based analysis allowed quantifying the decrease of the cross-correlation coefficient between the temperature increase of the machine's body and the power losses in the case of the elliptical magnetic motion field in the air-gap of the induction machine in comparison with the circular case. This phenomenon is due to

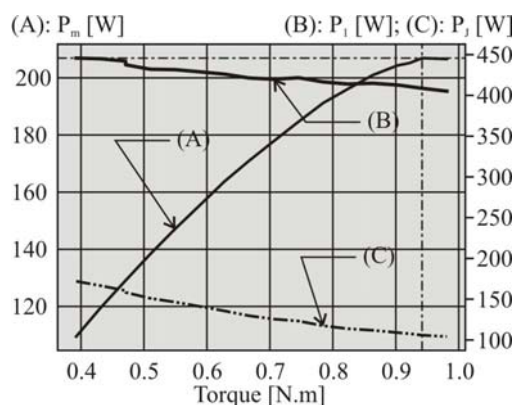


Fig. 10. Case 2 - $C = 11 \mu\text{F}$. The graphs of the mechanical power - P_m , the input power - P_i and the thermal power-losses - P_j versus the load's torque from the experimental data.

the stationary component of the field that separately heats the machine's body.

The proposed method is an alternative to the estimation of the shape - circular or elliptical - of the magnetic motion field in the air gap of the machine by means of the direct observations of the stator currents. This approach is load-dependent and therefore several equivalent parameters of the machine's model, such as the stator's resistances of the main and auxiliary phases and the equivalent resistance of the rotor must be taken into account. These parameters are temperature-dependent or non-observable and thus approximations must be made. In comparison, the proposed method addresses directly to the overheating of machine operating under circular or elliptical magnetic motion field. The estimations of the cross-correlation between the increase of temperature of the machine's body and the power-losses is addressed to the thermal model of the machine and onto the observations of the input power and the mechanical power of the machine.

This result proves to be important for the evaluation of the eccentricity of the magnetic motion field on test-benches and for the control of the electronically-switched capacitor in variable speed operation of the drive. Likewise, these results prove that promising results may be achieved in post-processing of field spectra estimations with the Finite Elements Method-based software environments.

Contribution of authors:

Danila Adrian - 70%

Campeanu Radu Mihai - 30%

Received on July 17, 2019

Editorial Approval on November 15, 2019

REFERENCES

- [1] G. Grellet, and G Clerc. *Actionneurs Electriques*, 2nd ed., Paris: Eyrolles, 2002, pp. 289-296.
- [2] E. Mechkov. "Application of infrared thermography technique in transformers maintenance in distribution network" *2017 15th International Conference on Electrical Machines, Drives and Power Systems (ELMA)* Sofia, Bulgaria, 1-3 June 2017, pp. 354-357.
- [3] A. G. Garcia-Ramirez, L. A. Morales-Hernandez, R. A. Osornio-Rios, A. Garcia-Perez, R. J. Romero-Troncoso. "Thermographic technique as a complement for MCSA in induction motor fault detection" *2014 International Conference on Electrical Machines (ICEM)*, Berlin, Germany, 2-5 Sept. 2014, pp. 1940-1945.
- [4] Danila A. "Experimental identification and accurate model validation of the thermal model of an electric machine based on the finite elements method," *Proceedings of the 16th Int. Conf. on System Theory, Control and Computing (ICSTCC)*, Sinaia, Romania, 12-14 Oct. 2012, pp. 1-6.
- [5] Danila A. "An Implementation of the Image Processing Techniques for the Thermal Field Analysis of the Induction Machines", *Proceedings of the 12th International Conference On Electromechanical And Power Systems (SIEMEN)*, Craiova, Romania-Chisnau, Rep. Moldova, 9-11 Oct. 2019.
- [6] Zhi-Pei Liang, and P.C. Lauterbur. *Principles of Magnetic Resonance Imaging. A Signal Processing Perspective*, New Jersey: IEEE Engineering in Medicine and Biology Society, 1999, pp. 36-44, 187-188.
- [7] Chernov N. *Circular and Linear Regression: Fitting Circles and Lines by Least Squares*, CRC Press, June 22 2010.
- [8] Stéfan van der Walt, Johannes L. Schönberger, Juan Nunez-Iglesias, François Boulogne, Joshua D. Warner, Neil Yager, Emmanuelle Guillard, Tony Yu and the scikit-image contributors. *Scikit-Image: Image processing in Python*, PeerJ 2:e453, 2014.